Separation and Purification Technology 380 (2026) 135455

Contents lists available at ScienceDirect

Separation and Purification Technology

journal homepage: www.elsevier.com/locate/seppur

Mechanistic insights for defluoridation of industrial wastewater by MIL-96 (Al) filters

Zhuang Liu [a,1], Xinyang Cai [f,1], Sandra Dirè [c,d], Emanuela Callone [c,d], Xiaolin Zhang [e], Jinming Luo [b], Francesco Parrino [c,*], Dawei Wang [a,*]

[a] Key Laboratory of Integrated Regulation and Resource Development of Shallow Lakes, Ministry of Education, College of Environment, Hohai University, Nanjing 210098, PR China.
[b] State Environmental Protection Key Laboratory of Environmental Health Impact Assessment of Emerging Contaminants, School of Environmental Science and Engineering, Shanghai Jiao Tong University, Shanghai 200240, PR China.
[c] Department of Industrial Engineering, University of Trento, via Sommarive 9, 38123 Trento, Italy.
[d] "Klaus Müller" Magnetic Resonance Lab., Department of Industrial Engineering, University of Trento, via Sommarive 9, 38123 Trento, Italy.
[e] State Key Laboratory of Pollution Control and Resource Reuse, School of Environment, Nanjing University, Nanjing 210023, PR China
[f] Jiangsu Nanda Huaxing Environmental Protection Technology Co., Ltd, Yancheng 224001, PR China.

ARTICLE INFO

Keywords:
Metal organic frameworks
Fluoride
Adsorption
Ion exchange
Coprecipitation
Magic angle spinning nuclear magnetic resonance

ABSTRACT

The rapid development of semiconductor and electronics industries have urged novel adsorbents for fluoride removal from wastewater. In this study, we developed a metal-organic framework filter by *in-situ* implanting MIL-96(Al) onto Al mesh, which demonstrated effective and stable fluoride removal over a wide range of pH (3−11). The solid state nuclear magnetic resonance (NMR) and X-ray photoelectron spectroscopy (XPS) results revealed that the different structural changes to which Al3 sites are subjected upon pH modifications trigger fluoride adsorption through Lewis interactions at acidic pH values and through ligand exchange mechanism at neutral/alkaline pH values. Moreover, the filter demonstrated limited Al ions leakage and satisfactory adsorption selectivity towards fluoride among chloride, nitrate, and sulfate, at concentrations up to 50-times higher than fluoride. As a proof of concept for practical applications, the developed filters were sealed in tandem into a home-made filter holder and tested for fluoride removal from real industrial wastewater. When 12 filters were used, fluoride concentrations decreased from 5.8 mg/L to below 1.5 mg/L after 10 min of hydraulic retention time in the filter holder over 5 consecutive cycles. We hope this work may provide new insights for the design of novel adsorbents for fluoride removal.

1. Introduction

The rapid development of photovoltaic and semiconductor industry has urged the upgrade of the treatment of fluoride-containing wastewater, and many countries improved their effluent standards for fluoride. For instance, the concentration limit of fluoride in the effluent has been upgraded to 2.0 mg/L since 2018 in India [1], and Jiangsu province in China has required that the fluoride in aqueous effluents cannot exceed 1.5 mg/L since 2022 [2]. Therefore, robust and efficient defluoridation technologies are urgently needed. To this aim, numerous approaches, such as precipitation [3], adsorption [4], electrodialysis [5], and membrane technology [6] have been proposed. Among them, adsorption is particularly promising for its cost-effectiveness, high efficiency, and robustness under a wide range of operating conditions [7]. Many adsorbent materials have been investigated for defluoridation, such as charcoal [8], carbon nanotubes [9], zirconium oxide [10], and bauxite [11]. Activated alumina (AA) has been among the most extensively studied and used ones, due to its satisfactory adsorption capacity and low cost [12]. However, AA can selectively remove fluoride through specific Lewis acid-base interactions [10], which are efficiently displayed only below the zero point charge value (pH < 6) [13,14]. Therefore, this material cannot be proposed to treat aqueous waste downstream to processes producing semiconductors, photovoltaic cells, non-ferrous metals, and organofluorine compounds, where typical pH values are often higher than 6 [15]. More importantly, AA is slightly soluble under acidic conditions, and the resulting release of Al ions in

* Corresponding authors.
E-mail addresses: francesco.parrino@unitn.it (F. Parrino), dawei.wang@hhu.edu.cn (D. Wang).
[1] These authors contributed equally.

https://doi.org/10.1016/j.seppur.2025.135455
Received 16 June 2025; Received in revised form 9 September 2025; Accepted 29 September 2025
Available online 30 September 2025

the aqueous stream poses relevant threats to the environment and to human health [16,17].

Within this context, it is urgently necessary to develop novel adsorbents for defluoridation to address the above limitations. Among all options, metal organic frameworks (MOFs) have gained increasing attention because of their large surface area and tailored surface functionalities [18]. For example, several Zr-based MOFs, have been applied for the defluoridation of water solutions and showed stable performances even in the presence of competing ions [19–21]. Also Al-based MOFs, such as AlFu MOF [22], MIL-53(Al) [23], showed high adsorption capability towards fluoride. However, a major disadvantage of these attempts is that MOFs have been applied in the form of small particles (usually in micrometer- or even smaller scale), which may pose threat to safety in the case of inefficient recovery. In addition, the small size of the particles facilitates their aggregation, resulting in a decrease of the active sites of the adsorbent and, eventually, in non-negligible efficiency losses. A green Al-MOF sample has been recently deposited onto activated carbons to face this issue, with excellent fluoride adsorption activity, which however strongly reduced after three adsorption/regeneration cycles [24].

A previous study has shown that powdered MIL-96(Al) was able to remove fluoride efficiently under a wide pH range (3−10), but the underlying mechanism remained uncovered [25]. Herein, for the first time MIL-96(Al) was grown on an aluminum mesh as the substrate. The resulting filter demonstrates high structural stability and robustness, thus addressing the concerns on inefficient recycling and aggregation of small powders. This filter also demonstrates high adsorption capacity and selectivity towards fluoride ions, and low Al leakage over a wide range of pH, showing promising properties for practical applications. Finally, a thorough structural characterization revealed some mechanistic insights underlying the satisfactory defluoridation performances maintained under a wide range of pH values.

2. Materials and methods

2.1. Chemicals and materials

Sodium fluoride (NaF, 99.00 %), *N*,*N*-dimethylformamide (DMF, 99.50 %), nitric acid (HNO_3, 67.00 %), hydrochloric acid (HCl, 37.00 %), sodium hydroxide (NaOH, 96.00 %), sodium nitrate ($NaNO_3$, 99.00 %), sodium sulfate (Na_2SO_4, 99.00 %) and sodium phosphate (Na_3PO_4, 99.00 %) were purchased from Sinopharm Chemical Reagent Co. Ltd. (Shanghai, China). Trimesic acid (1,3,5-btc, 98.00 %) was purchased from Aladdin Chemistry Co. Ltd. Aluminum mesh (10, 100, and 200 mesh, 99.50 % in purity) was obtained from Guantai Metal Materials Co. Ltd. (China).

2.2. Preparation of MIL-96(Al) filters

MIL-96(Al) was synthesized *in-situ* on an aluminum mesh by a hydrothermal method. Before the synthesis, the aluminum mesh (circle shape, diameter of 24 mm, mesh counts 100) was immersed into a sodium hydroxide solution (0.2 M) for 1 min to remove the oxides on its surface, rinsed with anhydrous ethanol, and dried under nitrogen flow. In a typical synthesis process, 1,3,5-btc (0.08 mM), HNO_3 (90 μL), and deionized water (10 mL) were mixed in a beaker and magnetically stirred until complete dissolution of 1,3,5-btc. The solution was then transferred into a Teflon-lined stainless-steel autoclave, containing the pretreated mesh. The autoclave was then sealed and maintained at 210 °C for 24 h. Once cooled down at room temperature, the filter was soaked in DMF, washed several times with deionized water, and then dried at 80 °C for 10 h.

2.3. Preparation of reference filters

Selected fluoride adsorption tests were carried out in the presence of two reference filters: the pristine aluminum mesh, treated as described above, and the aluminum mesh onto which Al_2O_3 was deposited by simply heating the mesh at 550 °C for 48 h. As shown in Fig. S1, the produced Al_2O_3 mesh showed aggregates of fused particles, whose primary size was of the order of tens of nanometers.

2.4. Characterization methods and analytical procedures

The produced MIL-96(Al) filter was characterized by X-ray diffraction (XRD, Ultima IV, Rigaku Corporation), scanning electron microscopy (SEM, S-4800, Hitachi), and X-ray photoelectron spectroscopy (XPS, ESCAlab 250, Thermofisher). The deposited MIL-96(Al) was then scratched from the Al mesh and the powder was further characterized by Brunauer-Emmett-Teller (BET) nitrogen physisorption (Micromeritics, ASAP 2020), zeta potential measurements (SurPASS 3, Anton Paar), and solid-state magic angle spinning (MAS) nuclear magnetic resonance (NMR, Bruker 400WB spectrometer).

A detailed description of the characterization methods is reported in the Supporting Information.

2.5. Adsorption and desorption experiments

Fluoride adsorption experiments were conducted in both batch and circulation modes. To determine the adsorption capacity of MIL-96(Al) and the effects of initial fluoride concentration, pH, and competing ions on the adsorption performance in batch mode, the produced MIL-96 (Al) was scratched off from the filter and transferred into beakers containing 80 mL of the fluoride solution. The magnetic stirring speed was set at 500 rpm, and the adsorbent dosage was 0.50 g/L. The fluoride concentration ranged between 5 and 20 mg/L. Samples of the dispersions were collected at specific time intervals and filtered (0.45 μm Nylon membrane, VWR). The concentration of fluoride was analyzed with a fluoride ion-selective electrode (PF-202, Leixian, calibration curve reported in Fig. S2). The concentration of released Al ions was measured using an inductively coupled plasma optical emission spectrometer (ICP-OES, Optima 8000, Perkin-Elmer). The adsorption capacity of the adsorbents for fluoride was calculated according to Eq. S1. Sodium hydroxide (0.20 M) and hydrochloric acid (0.20 M) solutions were used to adjust the initial pH. The influence of several interfering ions (nitrate, chloride, sulfate, and phosphate) was evaluated by adding different amounts of their sodium salts.

The applicability of the MIL-96(Al) grown onto the aluminum mesh, was demonstrated by performing fluoride adsorption in circulation mode, by using the experimental set-up shown in Fig. S3. Briefly, certain number of filters were sealed parallelly into a home-made filter holder, where fluoride-containing water (80 mL, was circulated by means of a submersible pump, 7 W, flow rate = 450 L/h). Both simulated wastewater (fluoride concentration was 10 mg/L) and real fluoride-containing industrial wastewater provided by an electronics manufacturing factory located in Jiangsu Province were tested.

The regeneration of MIL-96(Al), both deposited onto the aluminum mesh or as scratched powder, was carried out by immersing each filter or the recovered (by centrifugation) scratched powder in a NaOH solution (50 mL, 0.01 M) for 40 min, washing three times with deionized water, and finally drying them in an oven at 60 °C for 10 h.

3. Results and discussion

3.1. Characterization of MIL-96(Al)

A commercially available aluminum mesh was used as the substrate for the *in-situ* growth of MIL-96(Al), as described in the Experimental Part. As illustrated in Fig. 1A, the pristine Al mesh was grey. Closer observation using SEM showed that the surface of pristine Al mesh was flat, and the diameter of each Al wire was ~80 μm (Fig. 1B). After the growth of MIL-96(Al), yellow crystals were formed on the aluminum

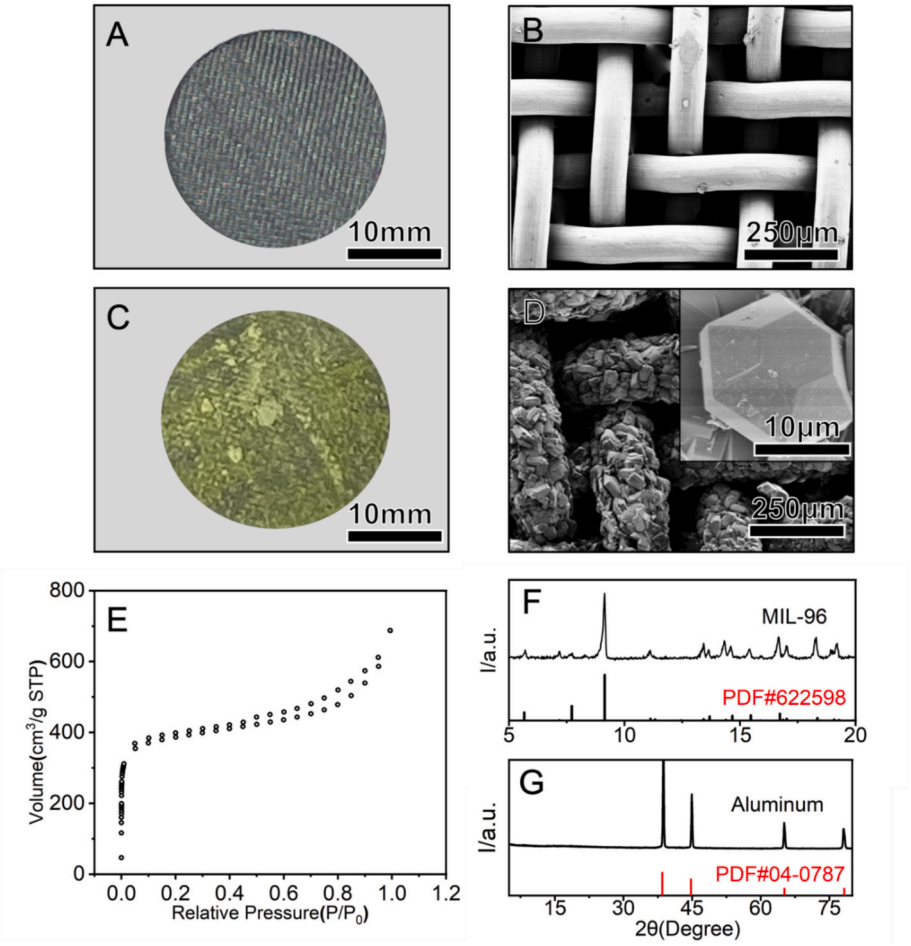

Fig. 1. Picture and SEM images of pristine aluminum mesh (A and B, respectively) and of the MIL-96(Al) filter (C and D, respectively). The inset in (D) is the zoomed SEM image. (E) N_2 sorption isotherms of MIL-96(Al). (F) XRD patterns of MIL-96(Al) and (G) the pristine aluminum mesh.

mesh (Fig. 1C), and the SEM images (Fig. 1D) showed that the aluminum wires were covered uniformly by crystals with truncated hexagonal pyramid morphology, which was consistent with previous studies [26]. To verify the composition and porous structure of the products, XRD and BET analyses were carried out directly on the filter and on the scratched powder, respectively. According to the BET analysis (Fig. 1E), the surface area of the synthesized product was 1486 m^2/g. The shape of the isotherm suggests the presence of microporosity and narrow-slit mesoporosity. The XRD patterns of the pristine Al mesh was consistent with that of metallic Al (PDF#04–0787, Fig. 1G), while the XRD patterns of the yellow crystals were consistent with that of MIL-96(Al) [27]. The loading of the MOF on the aluminum mesh was 0.87 ± 0.03 mg/cm^2. Some slight mismatch in the relative intensity of the retrieved patterns with respect to the reference can be attributed to the different growth procedure used in this work.

These results were further confirmed by multinuclear solid state NMR data. The ^{27}Al MAS NMR spectrum (Fig. S4) of MIL-96(Al) sample exhibits overlapped signals from 20 to −20 ppm, characterized by different chemical shifts and different quadrupolar parameters (Table S1) in the typical range of octahedral aluminum. The overall spectrum lineshape recalls that of $Al_{12}O(OH)_{18}(H_2O)_3(Al_2(OH)_4)[btc]_6{\cdot}24H_2O$, *i.e.* MIL-96, with few differences [28–30]. The three main components, namely Al1, Al2, Al3, are analogues to the ones found by Benzaqui et al., [28] thus confirming the production of the MIL-96(Al) structure. Al1 corresponds to an oxocentered trimer where every Al is coordinated to 4 bridging btc—O, one μ_3-O and one oxygen terminal ligand (OH or H_2O); Al2 coordinates 4 btc-O and 2 μ_2-OH and Al3 coordinates 2 btc-O and 3 μ_2-OH, both linked to form a 2D hexagonal network (Fig. S5).

Two other minor components (Al4 and Al5, the latter probably corresponding to an Al(V) site) were also detected, accounting for some structural defects that can arise from the employed synthesis conditions, thus justifying the differences respect to the published MIL-96 data [27,28]. In fact, Quintero-Alvarez et al. reported that even small changes in the synthesis route can produce significant structural changes [31].

The MIL-96 structure is confirmed also by the ^{13}C and ^{1}H MAS NMR spectra (see Fig. S6 and S7). The carbon spectrum of the as-synthesized sample, exhibits narrow carbon signals in both the aromatic (group of four resonances at 138.4, 134.5, 132.6 and 132 ppm) and carboxyl (170.5 ppm, corresponding to 2 inequivalent sites) region [30]. Finally, the lack of resonances above 10 ppm, in the proton spectrum indicates the complete deprotonation of the carboxylic functions, due to the full btc bonding to Al sites [31].

3.2. *Adsorption performance*

12 MIL-96(Al) filters were firstly sealed into a home-made filter holder to test their adsorption performance over fluoride in circulation mode (Fig. S3). The same number of pristine Al and Al_2O_3 filters were also tested for the sake of comparison. As shown in Fig. 2A, only approximately 20.9 % of fluoride (initial concentration 20 mg/L) was removed by the pristine Al mesh after 30 min and the removal rate remained steady for the next 330 min. It is worth noting that metallic aluminum can react with ambient oxygen and form a very thin layer of Al_2O_3 [32], which is amorphous [33] and difficult to be detected by XRD. Thus, the fluoride adsorption over the pristine Al mesh may be

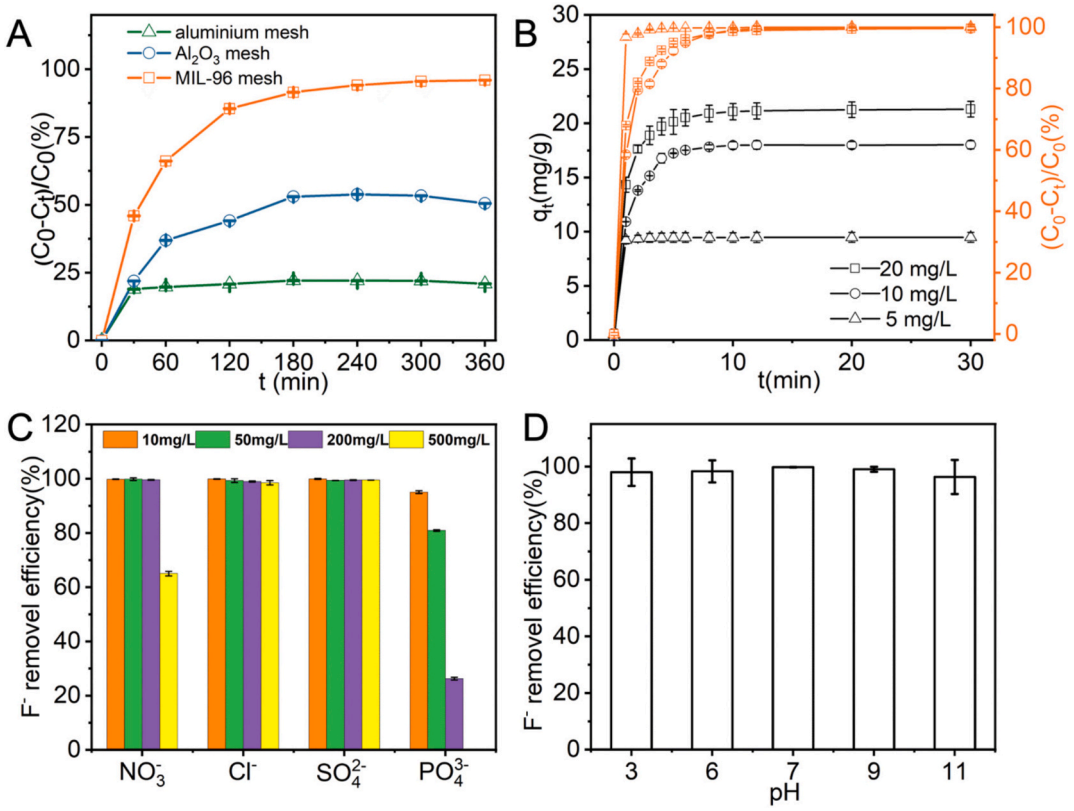

Fig. 2. Fluoride removal performance of (A) different filter types in recirculation mode (temperature = 298 K; pH = 7.0). (B—D) Adsorption of fluoride over the MIL-96(Al) powders that were scratched from the filters (temperature = 298 K; contact time = 4 h; MIL-96(Al) dose = 0.50 g/L, initial fluoride concentration = 10 mg/L): (B) Effects of contact time and initial fluoride concentration; (C) Effects of competing anions; (D) Effects of different pH values.

ascribed to the alumina produced on the surface of Al mesh.

In the presence of the Al_2O_3 filters, the removal rate of fluoride increased to 50.5 % during 360 min, thus confirming the fluoride adsorption capability of alumina elsewhere reported [34,35].

Notably, the removal efficiency of fluoride over the MIL-96(Al) filters reached approximately 96 % after 180 min and remained stable during the experiment. To further understand the outstanding adsorption features of MIL-96(Al) and to exclude the influence of the mesh on the adsorption performance of the MIL-96(Al) filters, a series of adsorption experiments were carried out by using the MIL-96(Al) scratched off from the Al mesh. The adsorption process was studied from both the kinetic and thermodynamic point of view. The adsorption of fluoride over MIL-96(Al) in batch mode as a function of the time of contact is reported in Fig. 2B for three different fluoride concentrations at pH 7. In all cases, the removal efficiency reached *ca.* 100 % after the first minutes. To reveal the apparent order of the adsorption rate with respect to the fluoride concentration, the curves were fitted by using pseudo-first-order and pseudo-second-order (Eq. S2-S3, Fig. S8) models. Unlike the pseudo-first order (Fig. S8A), the pseudo-second-order kinetic model (Fig. S8B) fitted satisfactorily the experimental values, and yielded R^2 values of 0.9999, 0.9924, and 0.9928 for the three initial fluoride concentrations of 5, 10, and 20 mg/L, respectively (Table S2). These results suggest that the adsorption of fluoride onto MIL-96(Al) may be triggered by chemisorption mechanisms [36], rather than by electrostatic interactions, in agreement with the NMR data reported below.

To get information on the thermodynamics of the fluoride adsorption process at pH 7, adsorption isotherms were obtained at three different temperatures as shown in Fig. S9. Both the Langmuir and Freundlich models were used to fit the experimental data, and the corresponding parameters are shown in Table S3. The Langmuir model (Eq. S4) fitted better than the Freundlich model (Eq. S5) for all of the studied temperatures, indicating that the adsorption may mainly take place onto sites, which are rather homogeneous in nature. The calculated maximum adsorption capacity of the MIL-96(Al) on the fluoride using the Langmuir model was 35.34 ± 1.68, 36.17 ± 2.41, and 36.99 ± 2.41 mg/g for 298, 308, and 318 K, respectively. These results were similar to those obtained in a previous study that demonstrated that MIL-96(Al) had a higher adsorption capacity than nano-alumina, mesoporous alumina, and granular zirconium-iron oxide [25].

We chose NO_3^-, Cl^-, SO_4^{2-}, and PO_4^{3-} as the interfering ions, since they are the most ubiquitous in the electronic industry wastewater and able to compete with fluoride for preferential adsorption onto the adsorbents [37]. The initial concentration of fluoride ions was 10 mg/L, and the concentrations of the added ions were varied from 10 to 500 mg/L. As shown in Fig. 2C, Cl^- and SO_4^{2-} had negligibly competing effects. In fact, even when the concentrations of these two ions were 500 mg/L (50 times the fluoride concentration), fluoride removal efficiency was only slightly inhibited. NO_3^- had little effects on the fluoride adsorption over a concentration ranging from 10 to 200 mg/L, but decreased the removal efficiency to 65 % when its concentration increased to 500 mg/L. This inhibitory effect of NO_3^- at high concentration can be attributed to its ability to form an outer-spherical complex with Al-OH on the material's surface [38]. PO_4^{3-} showed a considerable effect on fluoride adsorption. Already when PO_4^{3-} and fluoride concentration (10 mg/L) was the same, the removal rate of fluoride decreased to 95.05 %. When the concentration of PO_4^{3-} was increased to 500 mg/L, the adsorption of fluoride over MIL-96(Al) was completely inhibited. The competing electrostatic forces are not the major driving force since PO_4^{3-} (3/3.40) and F^-(1/1.33) have similar charge/radius ratios [39]. Instead, the complexation between PO_4^{3-} and Al may contribute to this inhibitory effect [40]. Meanwhile, as described in the later section, this inhibition can also be attributed to the buffering effect of phosphate.

We found that the removal rate of fluoride over MIL-96(Al) remained

almost unchanged over a wide range of pH (3–11), as shown in Fig. 2D. This feature was surprising, by considering that the performances of aluminum-based adsorbents (*e.g.* AA) are dramatically reduced at neutral/alkaline pH values. In fact, adsorption of fluoride onto AA is reported to be highly dependent on pH. We also found that the zeta potential values of MIL-96(Al) was also dependent on pH, being positive at pH = 3 but negative at pH = 5, 7, 9, and 11 (Fig. S10A). Moreover, according to the calculation based on Visual MINTEQ (Fig. S10B), fluoride in the solution is present as both HF and F^- (1:1) when the pH is lower than 3, and present as only F^- when the pH is higher than 5. The pH independent adsorption efficiency of fluoride, along with the previously mentioned phosphate inhibiting effect, suggest that the electrostatic force is not the major driving force for the adsorption of fluoride over MIL-96(Al). These findings induced us to provide additional evidences to reveal the adsorption mechanism of fluoride onto MIL-96(Al) under different pH values.

We finally investigated the regeneration performance of the scratched powders of MIL-96(Al). As shown in Fig. 3A, the removal rate of fluoride remained stable over five consecutive cycles, and approximately 85–90 % of fluoride could be desorbed after each cycle (Fig. 3B). Meanwhile, the XRD patterns (Fig. 3C) and morphology (Fig. 3D) of the regenerated MIL-96(Al) were similar to the pristine ones, indicating its stability and reusability. Table S4 depicts a comparative analysis of our study's results with the relevant existing literature. Considering desorption efficiency and decline of adsorption efficiency, it is worth mentioning that MIL-96(Al) has comparatively higher regeneration performances.

3.3. Adsorption mechanism

The stable adsorption performances of MIL-96(Al) over a wide range of pH values suggest that electrostatic forces could play a minor role. XPS spectra confirmed the presence of fluoride onto the MIL-96(Al) after the adsorption under all the studied pH conditions (Fig. S11A-C). In addition, compared to the pristine state, the binding energy of Al 2p shifted to higher energy positions after fluoride adsorption (Fig. S11D), indicating the formation of Al—F bonds [41].

XPS was used also to evaluate possible changes of MIL-96(Al) at different pH conditions. The O1s spectra recorded on the powders scratched from the filter both before (initial) and after pH adjustment, namely at acid (pH 3), neutral (pH 7) and alkaline (pH 11) conditions, are shown in Fig. 4A.

O1s XPS spectrum of MIL-96(Al) results from the convolution of three components attributed to Al—O (18.90 %), Al-OH (67.60 %) and H_2O (13.50 %). At pH 3, the decrease of Al—O bonds, and to a very minor extent of Al-OH, leads to water increase. At neutral conditions, Al—O disappears in favor of both Al-OH and H_2O, while at pH 11 the consumption of Al—O bonds contributes preferentially to the increase of the Al-OH component.

In agreement with XPS, ^{27}Al MAS NMR confirm the structural rearrangement upon changing the pH conditions even when fluoride was absent. As a matter of fact, the lineshape of ^{27}Al MAS NMR spectra (Fig. 4B) is clearly modified, particularly at basic pH. Fig. 4C displays the changes in linewidth of the different Al components, which account for the observed lineshape modifications.

Moreover, the results of the quantitative analysis performed on the Al spectra reveals that Al3 are the most sensitive sites, and experience a strong modification especially at basic pH. Fig. 4D displays the comparison of Al2 and Al3 (*i.e.* the sites belonging to the 2D hexagonal network, Fig. S5) respect to the other components: with respect to Al1 that remain almost insensitive to pH changes, Al3 component undergoes a progressive intensity reduction with a contemporary growth of Al4 and

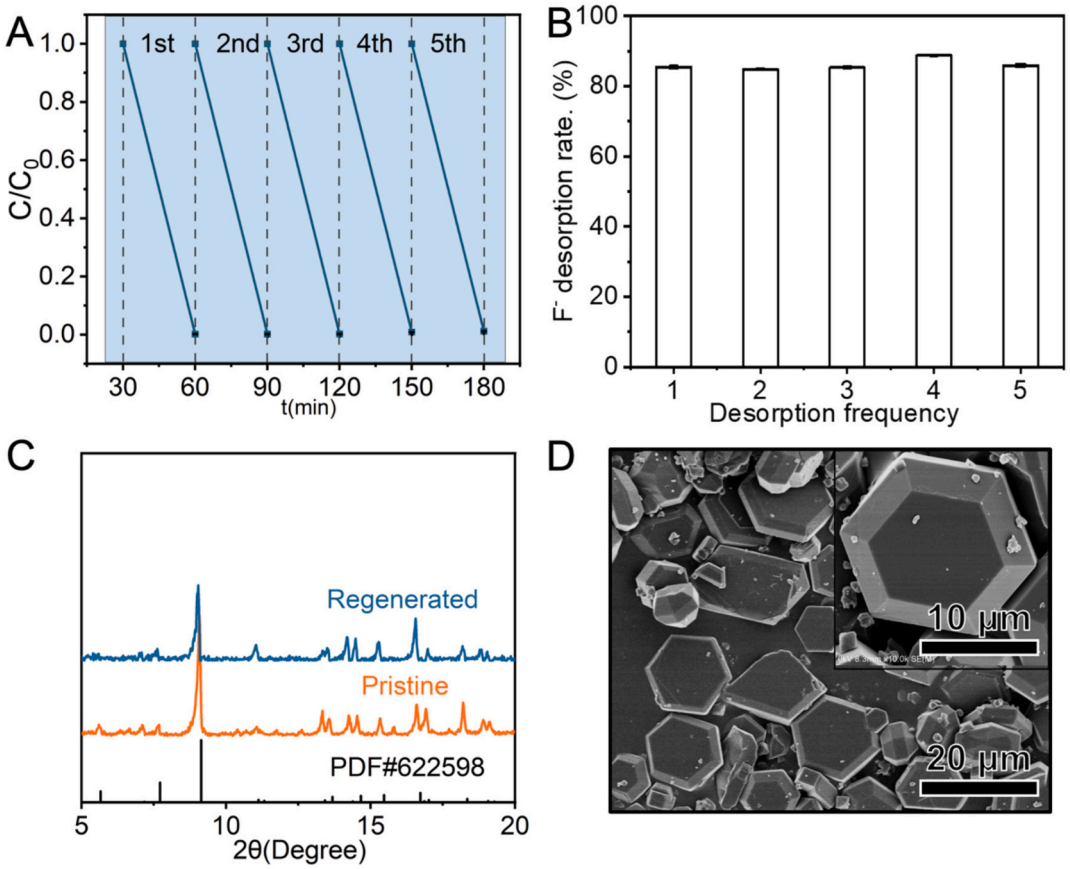

Fig. 3. Regeneration of the MIL-96(Al) scratched from the filters. (A) Recycle performance, (B) Desorption of fluoride, (C) XRD patterns and (D) SEM images of the regenerated MIL-96(Al).

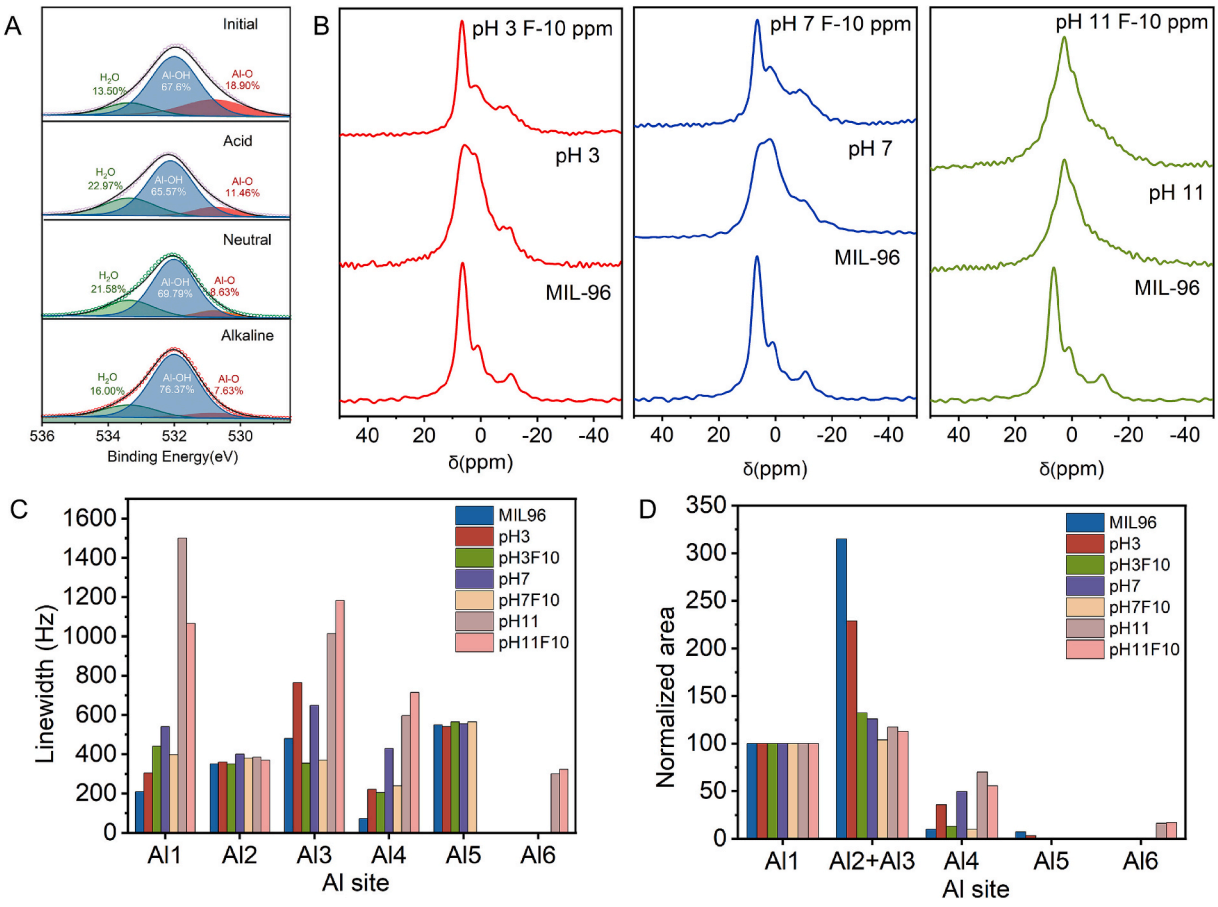

Fig. 4. (A) XPS spectra of O1s of MIL-96(Al) after pH adjustment and before fluoride adsorption. The binding energy for H_2O, Al-OH, and Al—O is 533.38, 532.08, 530.78 eV, respectively [42]. (B) ^{27}Al MAS-NMR spectra of MIL-96(Al) both after pH adjustment and fluoride adsorption. (C) Al linewidth changes at different conditions. (D) Relative amounts of the Al components with respect to Al1 area at different pH and after fluoride adsorption (for the sake of clarity, the sum of Al3 and Al2 areas are compared with the other components).

the appearance at pH 11 of a new component Al6 (a small resonance at 70 ppm). The appearance of Al6 suggested the production of a very low amount of Al(IV), that is typical of Al in highly basic environments [43]. This is consistent with a deterioration of the crystalline structure at pH 11, as suggested by the massive broadening of all the spectra with the formation of defective components, such as Al4 and Al6, and high disorder expressed by the strong increase of the linewidth of all Al sites (Fig. 4C).

Above results suggest that the Al3 sites belonging to the 2D hexagonal frame are the most involved ones in the structural reorganization highlighted by the XPS results (Fig. 4A). In particular, the μ_2-OH groups of the Al3 sites, at acidic pH can undergo protonation forming water, in agreement with XPS results. These reactions also leave unsaturated sites onto the participating Al centers, in agreement with the observed reduction of the amount of Al3 sites observed by NMR analysis. Under neutral and basic pH values, instead, the μ_2-OH groups of the Al3 sites can undergo the attack of hydroxyl anions forming Al-OH groups, in agreement with XPS results.

In support of these hypotheses, in the ^{13}C NMR spectrum (Fig. S12) the CH (b) resonance of the trimesate unit, which should be close to the Al3 sites, presents an upfield shift with increasing pH, thus indirectly demonstrating the transformation of μ_2-OH to Al-OH groups.

After fluoride adsorption, the ^{27}Al spectra show differences depending again on the pH conditions (Fig. 4B). The spectral features of MIL-96(Al) are generally recovered at pH 3 and 7 upon fluoride adsorption, suggesting an interaction between fluoride ions and the unsaturated sites formed upon protonation of Al3 centers. On the contrary, at pH 11 the recovery of fluoride ions does not alter significantly the disorder in the structure, indicating a competing ligand exchange process between F^- and OH^- at the Al sites.

To further confirm the proposed mechanism, we monitored the changes in the pH values of the suspension occurring after adding 0.50 g/L of MIL-96(Al) scratched from the filter as the adsorbent to three fluoride containing solutions at different initial pH values. When the initial pH was 3 (marked as Acid in Fig. 5), the pH of the solution slightly increased in the first 10 min and then remained almost unchanged. The initial pH increase can be justified by the mentioned protonation of the Al3 sites. The as formed unsaturated Al sites behave as Lewis acids, which can be neutralized by fluoride ions as a weak base. Therefore, at

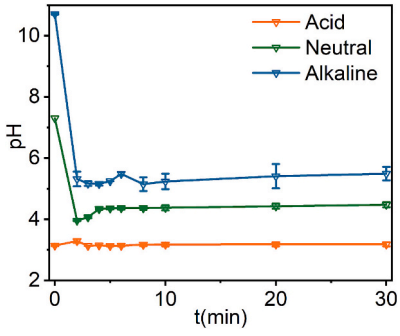

Fig. 5. pH changes during the fluoride adsorption under different initial pH (temperature = 298 K; MIL-96(Al) dose = 0.50 g/L, initial fluoride concentration = 10 mg/L).

acidic pH the fluoride adsorption did not significantly change the pH of the suspension, as it mainly involves the unsaturated Al sites created upon protonation of the μ_2-OH groups of Al3 sites.

When the initial pH was neutral or basic, a steep decrease of the suspension pH was observed soon after the addition of MIL-96(Al). This pH change can be ascribed to the consumption of the hydroxyl anions by μ_2-OH groups of the Al3 sites, which also produces Al-OH groups at the MIL-96(Al) surface. However, soon after, a slight increase of the pH, more pronounced under alkaline conditions, could be observed only in the presence of fluoride ions (Fig. S13). This pH increase in the presence of fluoride can be tentatively attributed to the release of OH anions in solution resulting from fluoride exchange reactions.

The above-proposed mechanism justifies the stable performances of MIL-96(Al) over a wide range of pH, due to the different adsorption mechanisms taking place at the different pH values. Moreover, it suggests that the inhibitory effect of PO_4^{3-} on fluoride adsorption observed at neutral pH could result from its pH buffering effect. Indeed, as shown in Fig. S14, when PO_4^{3-} was present even at a concentration of 10 ppm, the solution pH remained much more stable, thus inhibiting the hypothesized structural changes required for fluoride adsorption.

3.4. Real wastewater tests

We also used a real fluoride-containing wastewater to evaluate the application potentials of the developed MIL-96(Al) filters. The wastewater was collected from an electronic manufacturing factory located in Jiangsu Province (China), and its quality parameters are listed in Table S5. Specifically, the concentration of fluoride was 5.81 mg/L, and the concentrations of Cl^- and SO_4^{2-} were 774 and 803 mg/L, respectively. This wastewater also contained NO_3^- and PO_4^{3-} but with low concentrations (1.14 and 0.01 mg/L, respectively). Similar to the experimental set-up for the simulated wastewater, 12 MIL-96(Al) filters were sealed into the filter holder where the wastewater was recirculated. As shown in Fig. 6A, the concentration of fluoride decreased to 1.5 mg/L within 60-min operation, which represented ~10 min of hydraulic retention time (HRT, calculated according to Eq. S6) in the filter holder. This concentration meets the latest effluent standard of Jiangsu Province, which regulates the effluent concentrations of fluoride from the industries. We noted that the treatment time that required to meet the effluent standard varied exponentially with the number of MIL-96(Al) filters used. Specifically, it took ~20 min of HRT when only 6 filters were used, but less than ~5 min of HRT when 18 filters were used to meet the effluent standard.

The leaching of aluminum is a key indicator of the safety and environmental performance of aluminum-based adsorbents. Excessive aluminum leaching can lead to high concentrations of aluminum in water, which may have toxic and cumulative effects. These effects are harmful not only to plants and animals but can also cause various neurological disorders in the human central nervous system [44]. Therefore, the leakage of aluminum was also measured during the treatment of the real wastewater using MIL-96(Al) filters. For all the three experimental set-ups (6, 12, and 18 filters), the concentrations of aluminum increased with the treatment time but remained steady after 180 min of operational time. The final concentrations of aluminum were all below 1.5 mg/L. We also tested the recycling performances of the MIL-96(Al) filters towards the real wastewater and found that the removal efficiency of fluoride deteriorated slightly over the cycles (Fig. 6B). However, the concentration of fluoride recovered after each cycle to regenerate MIL-96(Al) was relatively stable after all the cycles (Fig. 6C). In addition, the SEM images (Fig. 6D) of the regenerated filters

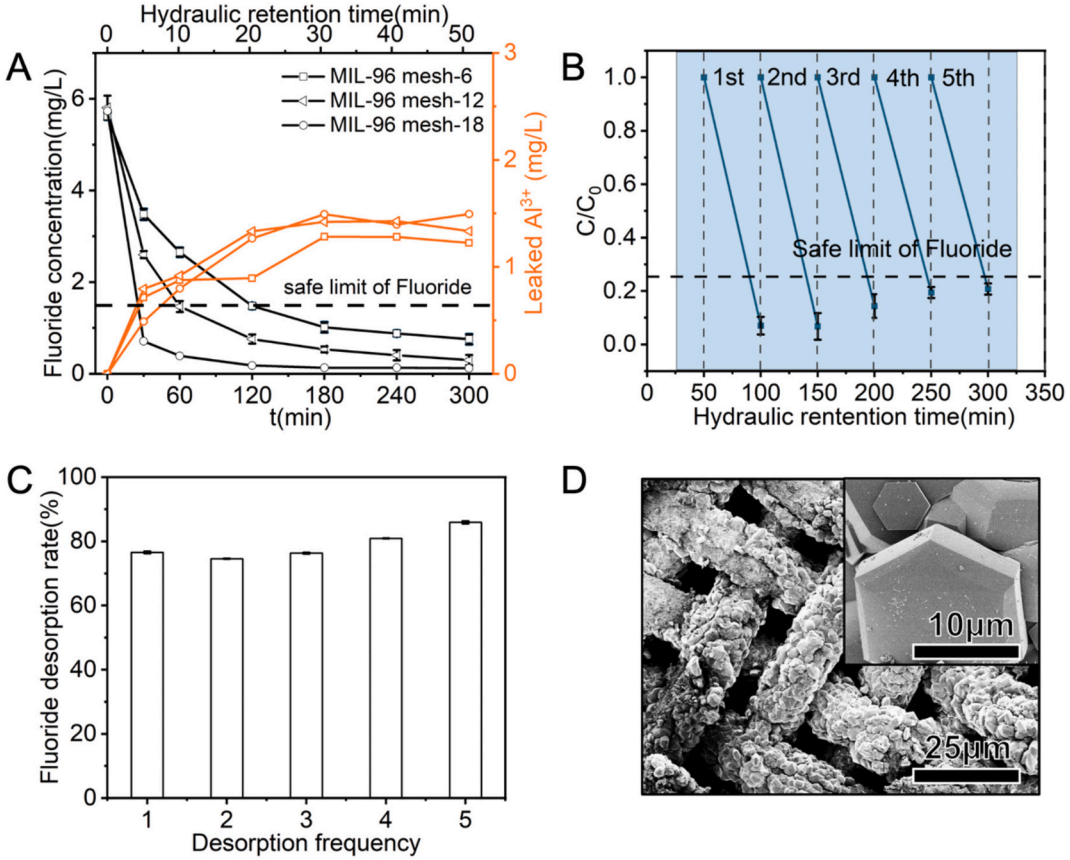

Fig. 6. Adsorption tests of real fluoride-containing wastewater. (A) The removal rate of fluoride with 12 pieces of MIL-96(Al) filters (black curves) and the corresponding leaked Al^{3+} concentrations (orange curves). (B) Regeneration test of the MIL-96(Al) filters. (C) The corresponded desorption of fluoride. (D) The SEM images of the regenerated MIL-96(Al) filter after 5-cycle use.

were identical to the pristine ones, suggesting the structural integrity of the filters. However, we noted that some crystals were physically detached when the filters were sealed in and out between different cycles. Thus, we ascribed the deteriorated performances over different cycles to the lower amount of MIL-96(Al) remaining after each cycle.

To further demonstrate the application potential of the developed MIL-96(Al) filters, we also fabricated filters from aluminum woven wire cloth with different mesh counts, as shown in Fig. S15A-C. Keeping constant the amount of filters sealed into the filter holder (12), the filters with more mesh counts (200 mesh) showed faster fluoride removal (Fig. S15D). The results showed in Fig. 6 and Fig. S15 demonstrate the application potentials of the developed MIL-96(Al) filters for the treatment of real industrial wastewater.

4. Conclusion

In this work, we report the MIL-96(Al) filters, which is synthesized with Al mesh as the substrate, for the removal of fluoride from real industrial wastewater. It is believed that the synthesis can be scaled up for real applications. Notably, our study revealed that MIL-96(Al) is subject to structural alterations in response to pH changes. The structural alterations result into two different adsorption mechanisms under acid and neutral/alkaline conditions, which enable the efficient fluoride removal under a wide pH range. We expect that the mechanisms revealed here can provide insights for the design of other MOFs-based adsorbents. Specifically, given that MOFs contains numerous metal sites, they may find broad applications as efficient adsorbents for the adsorption of fluoride in complex water matrices.

CRediT authorship contribution statement

Zhuang Liu: Writing – original draft, Methodology, Investigation. **Xinyang Cai:** Writing – original draft, Methodology, Investigation. **Sandra Dirè:** Writing – review & editing, Validation, Supervision, Conceptualization. **Emanuela Callone:** Visualization, Methodology, Investigation, Formal analysis, Data curation. **Xiaolin Zhang:** Writing – review & editing. **Jinming Luo:** Writing – review & editing, Funding acquisition. **Francesco Parrino:** Writing – review & editing, Supervision, Data curation, Conceptualization. **Dawei Wang:** Writing – review & editing, Writing – original draft, Supervision, Funding acquisition, Conceptualization.

Declaration of competing interest

The authors declare the following financial interests/personal relationships which may be considered as potential competing interests: Dawei Wang reports financial support was provided by National Natural Science Foundation of China. If there are other authors, they declare that they have no known competing financial interests or personal relationships that could have appeared to influence the work reported in this paper.

Acknowledgement

The authors would like to thank the financial support from the National Natural Science Foundation of China (52370072) and the Fundamental Research Funds for the Central Universities (B240203001).

Appendix A. Supplementary data

Supplementary data to this article can be found online at https://doi.org/10.1016/j.seppur.2025.135455.

Data availability

Data will be made available on request.

References

[1] C.F.Z. Lacson, M.-C. Lu, Y.-H. Huang, Fluoride-containing water: a global perspective and a pursuit to sustainable water defluoridation management -an overview, J. Clean. Prod. 280 (2021) 124236, https://doi.org/10.1016/j.jclepro.2020.124236.
[2] J.P. Environmental Protection Agency, China, Discharge standard of pollutants for municipal wastewater treatment plant, 2022.
[3] C. Yang, L. Guan, J. Wang, X. Yang, M. Lin, G. You, S. Tan, X. Yu, M. Ge, Enhanced fluoride removal behaviour and mechanism by dicalcium phosphate from aqueous solution, Environ. Technol. 40 (28) (2019) 3668–3677, https://doi.org/10.1080/09593330.2018.1484523.
[4] M. Zheng, J. Wang, D. Fu, B. Ren, X. Song, K. Kan, X. Zhang, Anchored growth of highly dispersed LDHs nanosheets on expanded graphite for fluoride adsorption properties and mechanism, J. Hazard. Mater. 442 (2023) 130068, https://doi.org/10.1016/j.jhazmat.2022.130068.
[5] F.D. Belkada, O. Kitous, N. Drouiche, S. Aoudj, O. Bouchelaghem, N. Abdi, H. Grib, N. Mameri, Electrodialysis for fluoride and nitrate removal from synthesized photovoltaic industry wastewater, Sep. Purif. Technol. 204 (2018) 108–115, https://doi.org/10.1016/j.seppur.2018.04.068.
[6] M.M. Damtie, Y.C. Woo, B. Kim, R.H. Hailemariam, K.-D. Park, H.K. Shon, C. Park, J.-S. Choi, Removal of fluoride in membrane-based water and wastewater treatment technologies: performance review, J. Environ. Manag. 251 (2019) 109524, https://doi.org/10.1016/j.jenvman.2019.109524.
[7] P. Mondal, M.K. Purkait, Preparation and characterization of novel green synthesized iron-aluminum nanocomposite and studying its efficiency in fluoride removal, Chemosphere 235 (2019) 391–402, https://doi.org/10.1016/j.chemosphere.2019.06.189.
[8] D.S. Bhargava, D.J. Killedar, Fluoride adsorption on fishbone charcoal through a moving media adsorber, Water Res. 26 (6) (1992) 781–788, https://doi.org/10.1016/0043-1354(92)90009-S.
[9] Y.-H. Li, S. Wang, X. Zhang, J. Wei, C. Xu, Z. Luan, D. Wu, Adsorption of fluoride from water by aligned carbon nanotubes, Mater. Res. Bull. 38 (3) (2003) 469–476, https://doi.org/10.1016/S0025-5408(02)01063-2.
[10] B. Pan, J. Xu, B. Wu, Z. Li, X. Liu, Enhanced removal of fluoride by polystyrene anion exchanger supported hydrous zirconium oxide nanoparticles, Environ. Sci. Technol. 47 (16) (2013) 9347–9354, https://doi.org/10.1021/es401710q.
[11] K. Cherukumilli, C. Delaire, S. Amrose, A.J. Gadgil, Factors governing the performance of bauxite for fluoride remediation of groundwater, Environ. Sci. Technol. 51 (4) (2017) 2321–2328, https://doi.org/10.1021/acs.est.6b04601.
[12] P. Loganathan, S. Vigneswaran, J. Kandasamy, R. Naidu, Defluoridation of drinking water using adsorption processes, J. Hazard. Mater. 248-249 (2013) 1–19, https://doi.org/10.1016/j.jhazmat.2012.12.043.
[13] A. Bhatnagar, E. Kumar, M. Sillanpää, Fluoride removal from water by adsorption—a review, Chem. Eng. J. 171 (3) (2011) 811–840, https://doi.org/10.1016/j.cej.2011.05.028.
[14] H. Qiu, M. Ye, M.-D. Zhang, X. Zhang, Y. Zhao, J. Yu, Nano-hydroxyapatite encapsulated inside an anion exchanger for efficient Defluoridation of neutral and weakly alkaline water, ACS ES&T Engineering. 1 (1) (2021) 46–54, https://doi.org/10.1021/acsestengg.0c00005.
[15] Y. Ku, H.-M. Chiou, The adsorption of fluoride ion from aqueous solution by activated alumina, Water Air Soil Pollut. 133 (1) (2002) 349–361, https://doi.org/10.1023/A:1012929900113.
[16] R.G. Miller, F.C. Kopfler, K.C. Kelty, J.A. Stober, N.S. Ulmer, The occurrence of aluminum in drinking water*, J. Am. Water Works Assoc. 76 (1) (1984) 84–91, https://doi.org/10.1002/j.1551-8833.1984.tb05267.x.
[17] D. Wang, S.C. Pillai, S.-H. Ho, J. Zeng, Y. Li, D.D. Dionysiou, Plasmonic-based nanomaterials for environmental remediation, Appl. Catal. B Environ. 237 (2018) 721–741, https://doi.org/10.1016/j.apcatb.2018.05.094.
[18] H. Furukawa, K.E. Cordova, M. O'Keeffe, O.M. Yaghi, The chemistry and applications of metal-organic frameworks, Science 341 (6149) (2013), https://doi.org/10.1126/science.1230444.
[19] K.-Y.A. Lin, Y.-T. Liu, S.-Y. Chen, Adsorption of fluoride to UiO-66-NH2 in water: stability, kinetic, isotherm and thermodynamic studies, J. Colloid Interface Sci. 461 (2016) 79–87, https://doi.org/10.1016/j.jcis.2015.08.061.
[20] F. Ke, C. Peng, T. Zhang, M. Zhang, C. Zhou, H. Cai, J. Zhu, X. Wan, Fumarate-based metal-organic frameworks as a new platform for highly selective removal of fluoride from brick tea, Sci. Rep. 8 (1) (2018) 939, https://doi.org/10.1038/s41598-018-19277-2.
[21] A. Ghosh, G. Das, Green synthesis of a novel water-stable Sn(ii)-TMA metal–organic framework (MOF): an efficient adsorbent for fluoride in aqueous medium in a wide pH range, New J. Chem. 44 (4) (2020) 1354–1361, https://doi.org/10.1039/c9nj05861c.
[22] S. Karmakar, J. Dechnik, C. Janiak, S. De, Aluminium fumarate metal-organic framework: a super adsorbent for fluoride from water, J. Hazard. Mater. 303 (2016) 10–20, https://doi.org/10.1016/j.jhazmat.2015.10.030.
[23] L. Huang, Z. Yang, S.I. Alhassan, Z. Luo, B. Song, L. Jin, Y. Zhao, H. Wang, Highly efficient fluoride removal from water using 2D metal-organic frameworks MIL-53 (Al) with rich Al and O adsorptive centers, Environmental Science and Ecotechnology. 8 (2021) 100123, https://doi.org/10.1016/j.ese.2021.100123.

[24] U.T. Uthappa, K.V. Ajeya, V. Sannasi, S.G. Lee, E.-H. Sohn, B.-J. Chang, I.-J. Park, J.H. Kim, M.D. Kurkuri, H.-Y. Jung, Green aluminum metal-organic frameworks (Al-MOFs) supported on commercial activated carbon for enhanced removal performances of industrial fluoride pollutants, J Water Process Eng 63 (2024) 105450, https://doi.org/10.1016/j.jwpe.2024.105450.
[25] N. Zhang, X. Yang, X. Yu, Y. Jia, J. Wang, L. Kong, Z. Jin, B. Sun, T. Luo, J. Liu, Al-1,3,5-benzenetricarboxylic metal–organic frameworks: a promising adsorbent for defluoridation of water with pH insensitivity and low aluminum residual, Chem. Eng. J. 252 (2014) 220–229, https://doi.org/10.1016/j.cej.2014.04.090.
[26] P. Geng, L. Wang, M. Du, Y. Bai, W. Li, Y. Liu, S. Chen, P. Braunstein, Q. Xu, H. Pang, MIL-96-Al for Li-S batteries: shape or size? Adv. Mater. 34 (4) (2022) e2107836 https://doi.org/10.1002/adma.202107836.
[27] T. Loiseau, L. Lecroq, C. Volkringer, J. Marrot, G. Férey, M. Haouas, F. Taulelle, S. Bourrelly, P.L. Llewellyn, M. Latroche, MIL-96, a porous aluminum Trimesate 3D structure constructed from a hexagonal network of 18-membered rings and μ3-Oxo-centered Trinuclear units, J. Am. Chem. Soc. 128 (31) (2006) 10223–10230, https://doi.org/10.1021/ja0621086.
[28] M. Benzaqui, R.S. Pillai, A. Sabetghadam, V. Benoit, P. Normand, J. Marrot, N. Menguy, D. Montero, W. Shepard, A. Tissot, C. Martineau-Corcos, C. Sicard, M. Mihaylov, F. Carn, I. Beurroies, P.L. Llewellyn, G. De Weireld, K. Hadjiivanov, J. Gascon, F. Kapteijn, G. Maurin, N. Steunou, C. Serre, Revisiting the aluminum Trimesate-based MOF (MIL-96): from structure determination to the processing of mixed matrix membranes for CO2 capture, Chem. Mater. 29 (24) (2017) 10326–10338, https://doi.org/10.1021/acs.chemmater.7b03203.
[29] C. Volkringer, D. Popov, T. Loiseau, N. Guillou, G. Ferey, M. Haouas, F. Taulelle, C. Mellot-Draznieks, M. Burghammer, C. Riekel, A microdiffraction set-up for nanoporous metal–organic-framework-type solids, Nat. Mater. 6 (10) (2007) 760–764, https://doi.org/10.1038/nmat1991.
[30] M. Haouas, F. Taulelle, C. Martineau, Recent advances in application of 27Al NMR spectroscopy to materials science, Prog. Nucl. Magn. Reson. Spectrosc. 94-95 (2016) 11–36, https://doi.org/10.1016/j.pnmrs.2016.01.003.
[31] F.G. Quintero-Álvarez, D.I. Mendoza-Castillo, C.K. Rojas-Mayorga, E. García-Hernández, I.A. Aguayo-Villarreal, A. Bonilla-Petriciolet, Mechanism, interfacial interactions and thermodynamics of the monolayer adsorption of trace geogenic pollutants from water using mil metal-organic frameworks: fluorides and arsenates, J. Mol. Liq. 380 (2023) 121665, https://doi.org/10.1016/j.molliq.2023.121665.
[32] T. Campbell, R.K. Kalia, A. Nakano, P. Vashishta, S. Ogata, S. Rodgers, Dynamics of oxidation of aluminum nanoclusters using variable charge molecular-dynamics simulations on parallel computers, Phys. Rev. Lett. 82 (24) (1999) 4866–4869, https://doi.org/10.1103/PhysRevLett.82.4866.
[33] C.C. Chang, D.B. Fraser, M.J. Grieco, T.T. Sheng, S.E. Haszko, R.E. Kerwin, R. B. Marcus, A.K. Sinha, Aluminum oxidation in water, J. Electrochem. Soc. 125 (5) (1978) 787–792, https://doi.org/10.1149/1.2131549.
[34] A. Bhatnagar, E. Kumar, M. Sillanpaa, Fluoride removal from water by adsorption-a review, Chem. Eng. J. 171 (3) (2011) 811–840, https://doi.org/10.1016/j.cej.2011.05.028.
[35] S. Jagtap, M.K. Yenkie, N. Labhsetwar, S. Rayalu, Fluoride in drinking water and defluoridation of water, Chem. Rev. 112 (4) (2012) 2454–2466, https://doi.org/10.1021/cr2002855.
[36] J. Song, S.A. Messele, L. Meng, Z. Huang, M. Gamal El-Din, Adsorption of metals from oil sands process water (OSPW) under natural pH by sludge-based biochar/chitosan composite, Water Res. 194 (2021) 116930, https://doi.org/10.1016/j.watres.2021.116930.
[37] Y. Qiu, L.F. Ren, L. Xia, C. Zhong, J. Shao, Y. Zhao, B. Van der Bruggen, Recovery of fluoride-rich and silica-rich wastewaters as valuable resources: a resource capture ultrafiltration-bipolar membrane Electrodialysis-based closed-loop process, Environ. Sci. Technol. 56 (22) (2022) 16221–16229, https://doi.org/10.1021/acs.est.2c04704.
[38] P.K. Singh, V.K. Saharan, S. George, Studies on performance characteristics of calcium and magnesium amended alumina for defluoridation of drinking water, J. Environ. Chem. Eng. 6 (1) (2018) 1364–1377, https://doi.org/10.1016/j.jece.2018.01.053.
[39] W. Tao, H. Zhong, X. Pan, P. Wang, H. Wang, L. Huang, Removal of fluoride from wastewater solution using Ce-AlOOH with oxalic acid as modification, J. Hazard. Mater. 384 (2020) 121373, https://doi.org/10.1016/j.jhazmat.2019.121373.
[40] B. Wan, R. Huang, J.M. Diaz, Y. Tang, Polyphosphate adsorption and hydrolysis on aluminum oxides, Environ. Sci. Technol. 53 (16) (2019) 9542–9552, https://doi.org/10.1021/acs.est.9b01876.
[41] R. Sun, H.-B. Zhang, J. Qu, H. Yao, J. Yao, Z.-Z. Yu, Supercritical carbon dioxide fluid assisted synthesis of hierarchical AlOOH@reduced graphene oxide hybrids for efficient removal of fluoride ions, Chem. Eng. J. 292 (2016) 174–182, https://doi.org/10.1016/j.cej.2016.02.008.
[42] A.V. Naumkin, A. Kraut-Vass, S.W. Gaarenstroom, C.J. Powell, NIST X-ray Photoelectron Spectroscopy Database, 2023, 2024.
[43] T.R. Graham, J.Z. Hu, N.R. Jaegers, X. Zhang, C.I. Pearce, K.M. Rosso, An amorphous sodium aluminate hydrate phase mediates aluminum coordination changes in highly alkaline sodium hydroxide solutions, Inorg. Chem. Front. 9 (24) (2022) 6344–6357, https://doi.org/10.1039/D2QI01642G.
[44] M. Corral-Bobadilla, A. González-Marcos, F. Alba-Elías, E. de Diez Santo Domingo, Valorization of bio-waste for the removal of aluminum from industrial wastewater, J. Clean. Prod. 264 (2020) 121608, https://doi.org/10.1016/j.jclepro.2020.121608.